minerals

MDPI

Article

Fluid Mixing, Organic Matter, and the Origin of Permian Carbonate-Hosted Pb-Zn Deposits in SW China: New Insights from the Fuli Deposit

Xingyu Liang [1], Bo Li [1,*], Xinyue Zhang [2], Huaikun Qin [3] and Gao Li [3]

[1] Faculty of Land Resources Engineering, Kunming University of Science and Technology, Kunming 650093, China
[2] Kunming Geological Prospecting Institute, China Metallurgical Geological Bureau, Kunming 650024, China; zxy3410@foxmail.com
[3] Fuli Pb-Zn Mine Co., Ltd., Fuyuan 655504, China; xvjiejz61237@163.com (H.Q.); wlyk913859@163.com (G.L.)
* Correspondence: 20163129@kust.edu.cn

Abstract: The Fuli Pb-Zn deposit is situated at the southwestern margin of the Yangtze Block in Yunnan. The deposit, which is hosted in the Permian Yangxin Formation dolomite, is a recent discovery. Our study indicates a significant presence of fluid inclusions in sphalerite from the Fuli Pb-Zn deposit, with fewer inclusions observed in dolomite and calcite. We conducted comprehensive petrographic, microthermometric, and laser Raman analyses on the inclusions within sphalerite and dolomite. Additionally, six samples of dolomite from the mineralization period were selected for H-O isotope analysis. The results of our study reveal the characteristics of ore-forming fluids and explore the mechanisms of ore formation. The study results indicate that the Fuli Pb-Zn deposit is a low- to medium-temperature hydrothermal deposit with fluid inclusions mainly composed of two-phase gas-liquid inclusions. Salinity and homogenization temperature analyses affirmed that there are two types of fluids present, one with low salinity and the other with high salinity. Laser Raman tests demonstrated the presence of CH_4, N_2, and CO_2 in the gas phase of the inclusions. Microthermometric analyses indicated that the sphalerite ore-forming fluids consist of a multicomponent system of Mg^{2+} and Ca^{2+} enriched fluids. The features of the ore-forming fluids in the Fuli deposit arise from a blend of high-temperature, low-salinity metamorphic fluids and low-temperature, high-salinity basin brines. The basin brines in question have the potential to emanate from the Youjiang Basin. The formation of the ore is ascribed to the TSR and the mixing of fluids. The combination of these processes provided the requisite materials (SO_4^{2-}), catalysts (Mg^{2+}), and reducing agents (organic matter, CH_4, and H_2S) required to initiate the thermochemical sulfate reduction (TSR). As the TSR proceeded, it caused a shift in the pH of the fluids, thus promoting the precipitation of metal sulfides.

Keywords: fluid mixing; organic matter; carbonate-hosted Pb-Zn deposits

Citation: Liang, X.; Li, B.; Zhang, X.; Qin, H.; Li, G. Fluid Mixing, Organic Matter, and the Origin of Permian Carbonate-Hosted Pb-Zn Deposits in SW China: New Insights from the Fuli Deposit. *Minerals* **2024**, *14*, 312. https://doi.org/10.3390/min14030312

Academic Editors: Maria Boni and Ryan Mathur

Received: 1 December 2023
Revised: 21 February 2024
Accepted: 13 March 2024
Published: 15 March 2024

1. Introduction

The southwestern edge of the Yangtze block is a renowned Pb-Zn mineralization zone in China (Figure 1), covering an area of around 170,000 square kilometers. Over 400 Pb-Zn deposits have been discovered within the triangular area made up of southwestern Sichuan, northeastern Yunnan, and northwestern Guizhou [1–4], making it an essential low-temperature hydrothermal metallogenic region of southern China. The Fuli Pb-Zn deposit is situated in the southeastern part of the southwestern margin of the Yangtze block (Figure 1). The deposit's ore bodies are layered and appear in the fractured zone of the Permian Yangxin Formation limestone. Prior reports and studies on the deposit focused mainly on its geological features, rock geochemistry, and isotope geochemistry. However, this investigation discovered significant hydrothermal mineralization in the deposit, which is also abundant in organic matter. The investigation of fluid inclusions in minerals is a vital

aspect of research on deposits. Various metallic deposits exhibit distinct fluid characteristics that aid in ore formation [5,6]. Nonetheless, there is a scarcity of research on the fluid inclusions of this deposit. The correlation between organic-rich fluids and mineralization has always been a topic of great interest among scholars in the field [7–9]. Numerous research studies have demonstrated the close association between metallic deposits and organic-rich fluids, often found in basins or basin margins. These deposits are genetically linked with organic matter, which plays a vital role in activating, extracting, migrating, and depositing metallic elements throughout the various stages of mineralization. Therefore, this study aimed to conduct systematic petrographic and microthermometric analyses on fluid inclusions, with a focus on the Fuli deposit. Laser Raman testing and isotopic analyses of H and O were utilized to summarize the characteristics of the ore-forming fluids in the Pb-Zn deposits and investigate the correlations between the organic matter, mineralization, and ore-forming fluids in the study region.

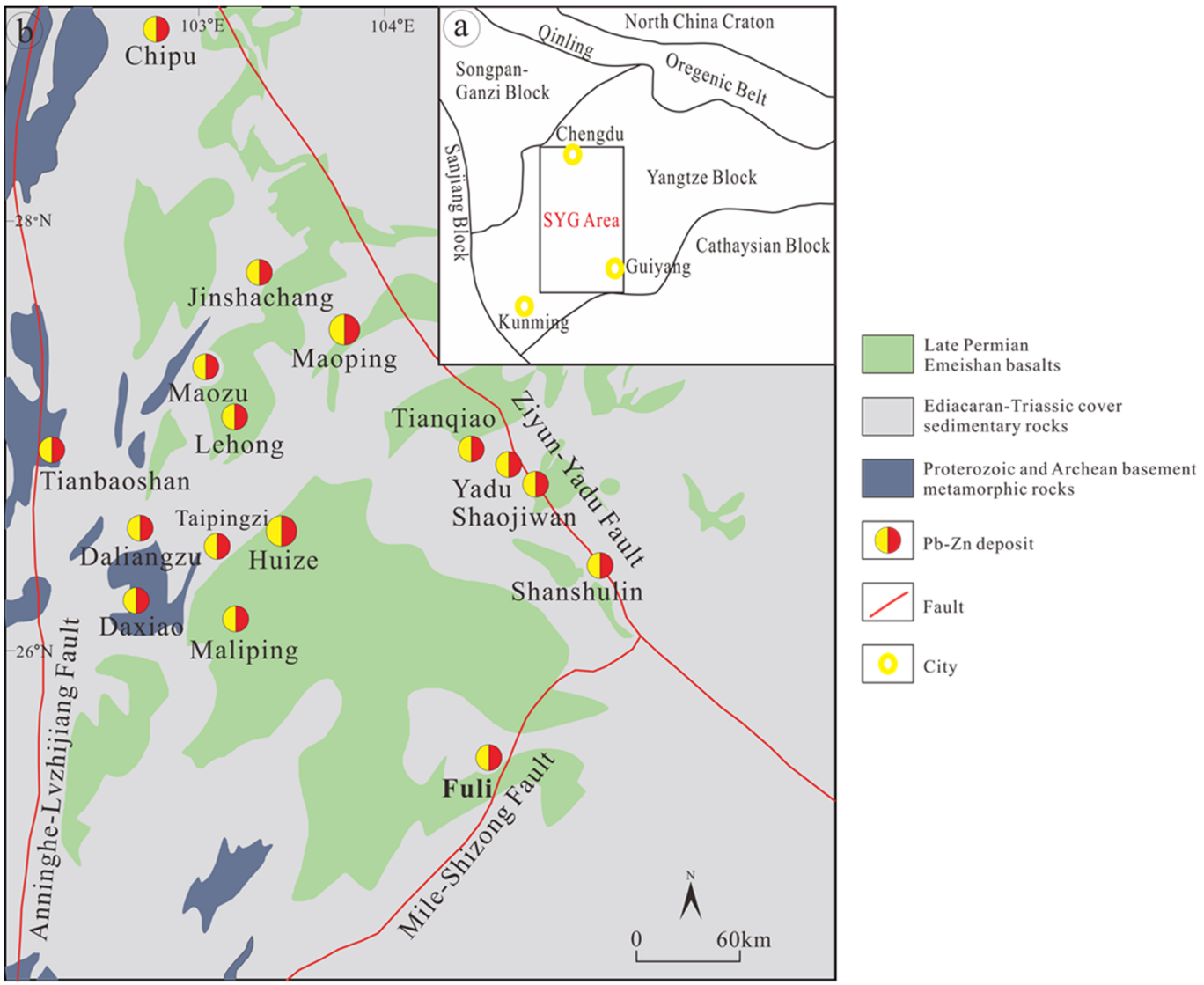

Figure 1. (**a**) Simplified geological framework of SW China showing the SYG province. (**b**) A sketched geological map of the SYG metallogenic province showing the distribution of Pb-Zn deposits and Emeishan basalt and the location of the Fuli deposit (modified from Han et al. [10,11], Zhou et al. [12], and Ren et al. [3]).

2. Geological Setting of the Region and Deposit

2.1. Geological Setting of the Region

The southwestern margin of the Yangtze block borders the southwestern Sanjiang orogenic belt (SB), northwestern Songpan–Ganzi orogenic belt (SGB), northern Qinling–Dabie orogenic belt (QDB), and southern Huaxia block (CB). It is limited by the northeast-trending Mile–Shizong–Anshun (MSA) fault, northwest-trending Kangding–Ziyun–Yadu (KYZ) fault, and north-directed Anning River–Luzhijiang (AL) fault. This region has experienced numerous tectonic events, magmatic occurrences, and metamorphic deformations. The stratigraphy primarily comprises metamorphic basement and sedimentary cover layers. The sedimentary cover layers mainly comprise Paleozoic, Mesozoic, and Cenozoic sedimentary rocks, predominantly marine carbonate rocks. The junction of the sedimentary blanket layers and the underlying basement exhibits an angular unconformity, whereas the connections between distinct stratigraphic units display either conformable or parallel unconformities.

2.2. Deposit Geology Setting

2.2.1. Tectonic Features

The Fuli Pb-Zn deposit is located between the Qujing Fault and the Mile–Shizong Fault (Figure 1). The basement in the study area is represented by the Middle to Late Proterozoic Kunyang Group, which is exposed only in the southwestern part of the study area [13]. The sedimentary record is missing from the Sinian to the Silurian period above it. The Middle Devonian Haikou Formation directly contacts the Kunyang Group with an angular unconformity. The Paleozoic tectonic events mainly had an east–west orientation. After several movements, including the Jinning Movement, Caledonian Movement, and Hercynian Movement, the regional tectonics changed to a north–south orientation as the main trend, followed by a northeast trend. After the tectonic movements of the Yanshan and Himalayan orogeny periods, the study area developed a north–south structural pattern as the dominant trend, with a secondary northeast trend, as well as east–west and north–west structures [14]. The sedimentary rocks in the study area include Proterozoic and Paleozoic carbonate and clastic rocks with a total thickness of more than 10,000 m, indicating long-term basin sedimentation. The development of the stratigraphy from Cambrian to Permian is relatively extensive but intermittent. During the Late Hercynian Movement, large-scale magmatism occurred in the region, consisting only of eruptions of basalt lava. The structural framework is characterized by parallel and nearly equidistant north–south trending faults. The northeast-trending structures are also well defined, large in scale, and have a long history. The north–south and northeast-trending structures play an important controlling role in the formation, distribution, and enrichment of zinc-lead mineralization in the area [12].

The northeast-trending Mile–Shizong Fault is the major fault in the area. Several gentle anticlines, synclines, and steep reverse fault structures are distributed throughout the study area. The distribution of regional stratigraphy, secondary structures, and mineralization is controlled by faults and folds. Together, the faults and folds control the distribution of regional stratigraphy, as well as the distribution of secondary structures and mineralization in the area [14].

2.2.2. Stratigraphy and Lithology

The study area's exposed stratigraphy consists of the Lower Permian Liangshan Formation, Middle Permian Yangxin Formation, Upper Permian Emeishan Formation, Lower Triassic Yongningzhen Formation, and Feixianguan Formation (Figure 2A). The ore-bearing formation in the deposit is the Permian Yangxin Formation (P_2y), which is mainly made up of interbedded dolomite and limestone and can be divided into three units (Figure 2B). The lower unit (P_2y^1) comprises light gray limestone. The middle unit (P_2y^2) contains interbedded light gray limestone and dolomite, with siliceous dolomite being localized and serving as the primary ore-bearing unit at the deposit. The upper unit (P_2y^3)

is made up of gray or dark gray thinly bedded dolomite, interbedded with gray or off-white dense limestone. The Emeishan Formation is an assemblage of dense massive basalt and tuffaceous basaltic breccia. The Yongningzhen Formation and Feixianguan Formation in the Lower Triassic consist of alternating layers of mudstone, limestone, and shale.

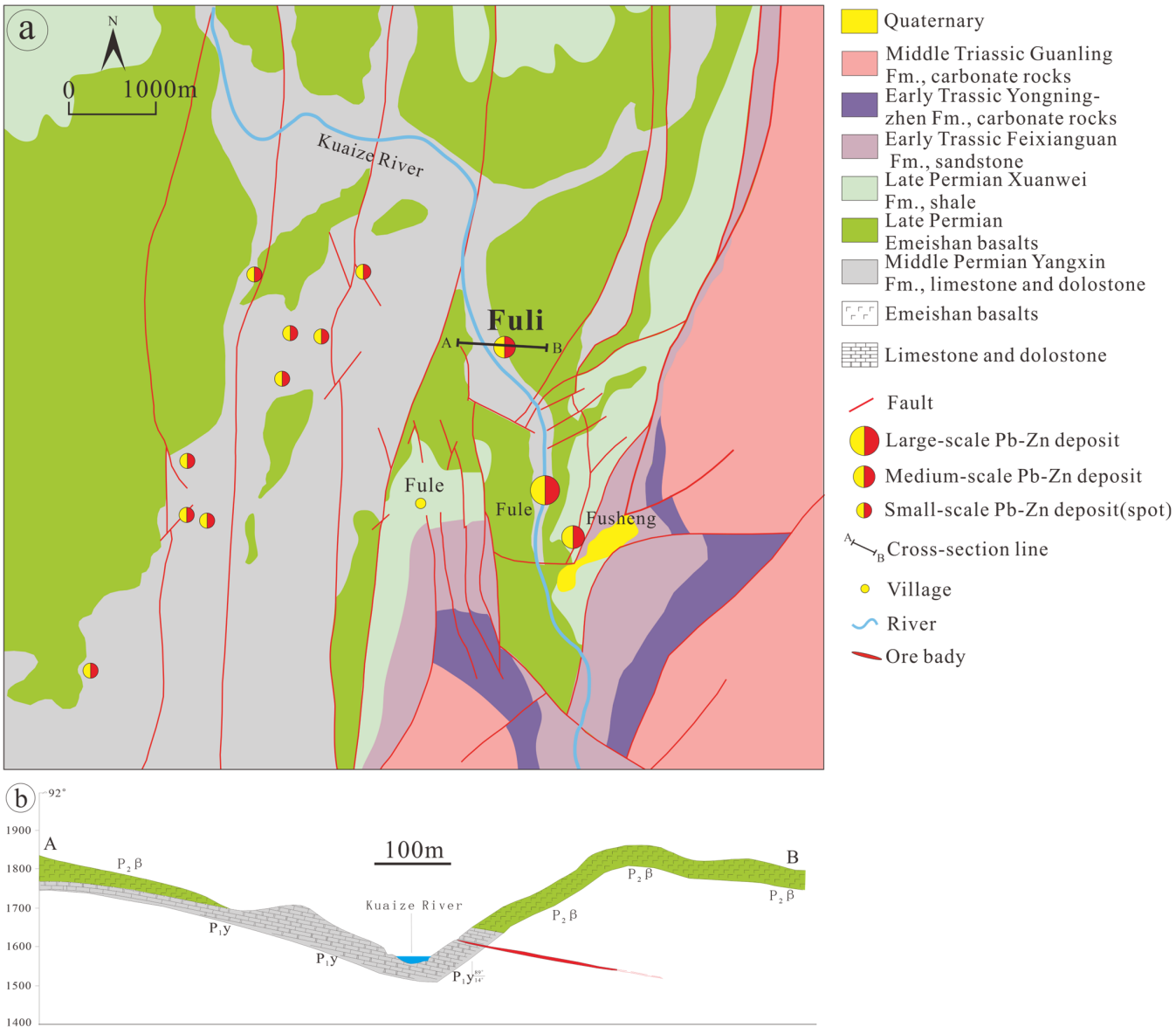

Figure 2. (**a**) Geological sketch map of the Fuli Pb−Zn deposit (modified from Zhou et al. and Ren et al. [2,3]). (**b**) A-B cross-section of the Fuli deposit.

2.2.3. Ore Bodies

The Fuli Pb-Zn deposit comprises two ore bodies situated within dolomitic limestone (Figure 2b), having a Pb+Zn grade of over 25%. The largest ore body is around 320 m long, 210 m wide, and has a thickness of roughly 1.2 m. It dips at a 15° angle towards the southeast and is thicker in the middle while being thinner at both ends. The ore body at the shallow part of the Fuli Pb-Zn deposit is relatively thin and has a lower content of metals. As depth increases, the ore body gradually becomes thicker, and the content of Zn and Pb increases.

2.2.4. Petrography and Mineralogy

Based on field observations, mineral assemblages, and preliminary lithological studies, the formation of the deposit can be classified into three stages: early mineralization, main mineralization, and post mineralization. Dolomite is the primary gangue mineral in the deposit, and all were formed by hydrothermal activity (Figures 3 and 4).

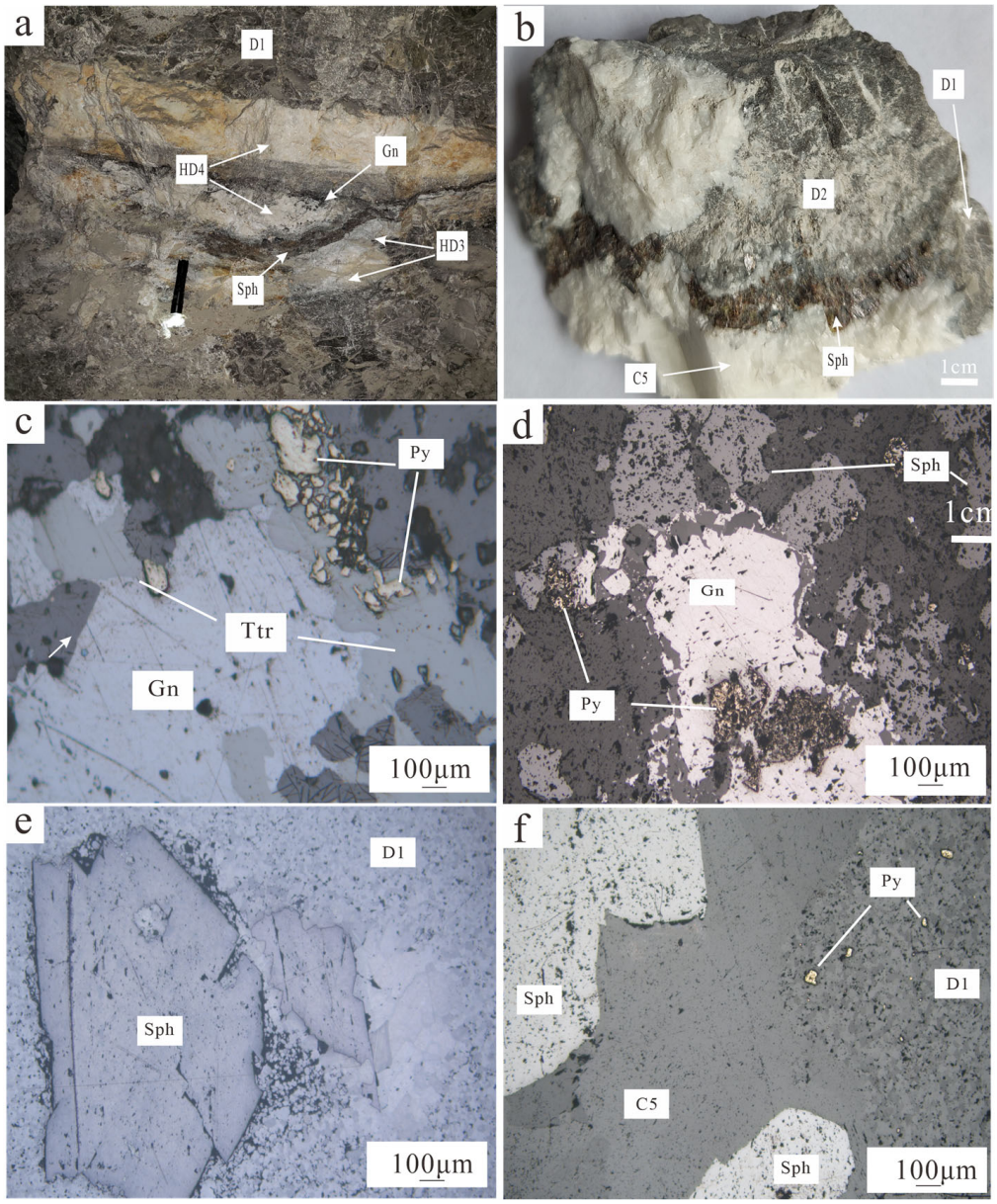

Figure 3. Photographs of the field and specimen studied and its textures from the Fuli Pb-Zn deposit. (**a**) Massive Sp are cemented by Cal veins. (**b**) Sphalerite veins filled in dolomite fissures. (**c**) Galena metasomatic pyrite and tetrahedrite. (**d**) Metasomatic relict pyrite and xeno-morphic sphalerite in an anhedral sphalerite fracture. (**e**,**f**) Sphalerite and dolomite with a granular structure.

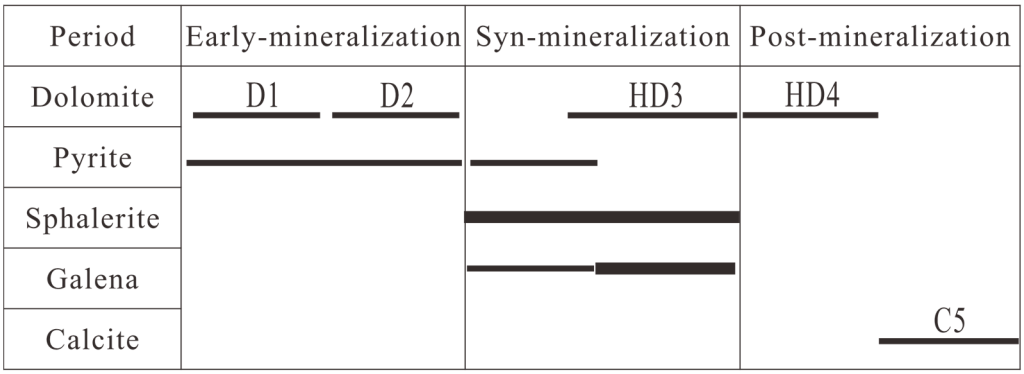

Figure 4. Mineral paragenesis in the Fuli Pb-Zn deposit.

(1) Early-Mineralization Stage: The primary characteristic of the ore in the early-mineralization stage includes the presence of two different types of hydrothermal dolomitization: D1 and D2. D1 dolomite is gray-black with irregular, fine-grained particles that are typically cemented by mineralizing gray dolomite. Conversely, D2 dolomite is gray-white with coarse-grained particles, featuring a white core and a dark gray-to-gray-white edge (Figure 3a). Blocky or impregnated sphalerite and galena have been discovered as replacements within the dolomite (Figure 3b).

(2) Main Mineralization Stage: This stage entails minerals forming within interlayer fractured zones, following the stratigraphic trend. Primarily, the main minerals are vein-like, impregnated, or blocky sphalerite, whereas galena appears in cubic crystals. Overall, sulfides display granular structures (Figure 3e,f) and replacement structures (Figure 3c,d), some of which form blocky or conglomerate-like structures, with impregnated structures present as well (Figure 3b). At this stage, sphalerite can be divided into two mineralization phases: Phase I sphalerite appears predominantly reddish brown to dark-brown in transmitted light, with mainly euhedral-to-subhedral crystals, while Phase II sphalerite appears predominantly brownish yellow to white in transmitted light, with mainly subhedral-to-anhedral crystals. The HD3 dolomite is a grey-white, meso-coarse-grained semi-autotype dolomite with a grain size ranging from 0.1 to 0.8 mm; it is distributed along the edges of sphalerite and galena and directly contacts or replaces wall rock.

(3) Post-Mineralization Stage: The HD4 dolomite often appears as saddle-like, euhedral coarse crystals that are white-milky white in color. It fills open spaces or cement fissures and is mostly in contact with the grey dolomite, and it was formed later than the grey dolomite. Coarse, vein-like calcite (C5) forms during the post-mineralization stage and envelops the sphalerite and galena from the main mineralization stage (Figure 3b,f).

3. Materials and Methods

3.1. Fluid Inclusion Microthermometry

All fluid inclusion microthermometric measurements were conducted at Nanjing University's State Key Laboratory for Mineral Deposits Research in China using the Linkam THMS600 heating–cooling stage installed on an Olympus BX-51 microscope (Tokyo, Japan). The Linkam THMS600 stage was calibrated by measuring the melting points of pure CO_2 (−56.6 °C) and pure water (0 °C), as well as the critical point of pure water (374.1 °C). The cooling and heating stages were calibrated over a temperature range of −195 °C to 600 °C, with uncertainties of around ±0.2 °C and ±2 °C, respectively [15].

The salinities of fluid inclusions lacking or having relatively low amounts of CO_2 were determined by the final melting of ice. All inclusions were cooled to below −120 °C to ensure unobstructed observations of the phase transition temperatures. Density calculations were conducted using the MS Excel 2010 (Redmond, WA, USA) spreadsheet "HOKIEFLINCS_H2O-NACL" [16] and Excel VBA macros to calculate the compositions of

the H2O-NaCl-CaCl2 fluid inclusions [17]. FIA (Fluid Inclusion Assembly) averages with 1σ uncertainties were used to report the temperatures, salinities, and densities.

3.2. H-O Isotope Analysis

Six samples of dolomite were selected for H-O isotope analysis at the analytical laboratory of the China National Nuclear Corporation Beijing Research Institute. The H-O isotope composition was analyzed using a Finnigan MAT253-EM mass spectrometer. The oxygen and hydrogen isotopic compositions were determined using the traditional BrF5 method and obtained from the FIs in dolomite, respectively. The details of this process were described by the authors of [18]. The H-O isotope values were standardized against the Vienna Standard Mean Ocean Water (V-SMOW). The δ18O analytical precision exceeded 0.2‰, and the δD analytical precision was better than 2‰. $\delta^{18}O_{fluid}$ was calculated using the formula in [19].

3.3. Laser Raman

Laser Raman spectroscopy was conducted at the State Key Laboratory for Mineral Deposits Research, Nanjing University, China, using a Renishaw RM-2000 laser Raman spectrometer. The experiment utilized a 514.5 nm argon ion laser as a light source. The laser was equipped with a slit width of 25 μm and operated with an exposure time of 30 s. The scanning range extended from 1000 to 4100 cm^{-1}.

4. Results

4.1. Characteristics of Fluid Inclusions

Fluid inclusions were prominently observed in sphalerite samples and more rarely in dolomite and calcite (Figure 5a–f). The primary fluid inclusions showcased lengths ranging from 4 to 25 μm and manifested in various shapes, like negative crystal, elliptical, circular, rectangular, and irregular shapes. The secondary fluid inclusions, on the other hand, were smaller in size (1–6 μm) and had mainly circular or irregular shapes, as shown in Figure 5b. Furthermore, primary FIAs were discovered throughout the sphalerite's growth zonation (Figure 5a,b). The inclusions in dolomite and calcite, ranging in size from 2 to 8 μm, are in negative crystal, elliptical, and rectangular shapes. The inclusions' phase types at room temperature (20 °C) were used to divide the fluid inclusions into three groups:

1. Liquid-rich fluid inclusions: This group included inclusions consisting of a liquid and vapor (L+V-type) (Figure 5a–h): These inclusions included more than 50% liquid phase and contained both gas and liquid phases. The fluid inclusions displayed diverse shapes, such as negative crystal, rectangular, and irregular shapes, with occasional elliptical and circular forms. Approximately 95% of all inclusions in this group were measured within 1–25 μm. The gas phase content of these inclusions ranged between 5% and 40%. Upon heating, the inclusions homogenized into a liquid phase, primarily consisting of H_2O.
2. Pure gas inclusions (V type) (Figure 5f): The inclusions observed were clusters of single-phase vapor, ranging in size from 1 to 5 μm, and commonly coexisted with the L+V-type inclusions.
3. Daughter mineral-bearing fluid inclusions: These rare multiphase inclusions contained gas, liquid, and solid phases and showed near-elliptical or irregular shapes (Figure 5c). Their sizes ranged from approximately 5 to 20 μm. The daughter minerals frequently exhibit a cubic crystal morphology, which may suggest the existence of NaCl minerals and indicate the presence of high-salinity elements in the ore-forming fluids of the Fuli deposit.

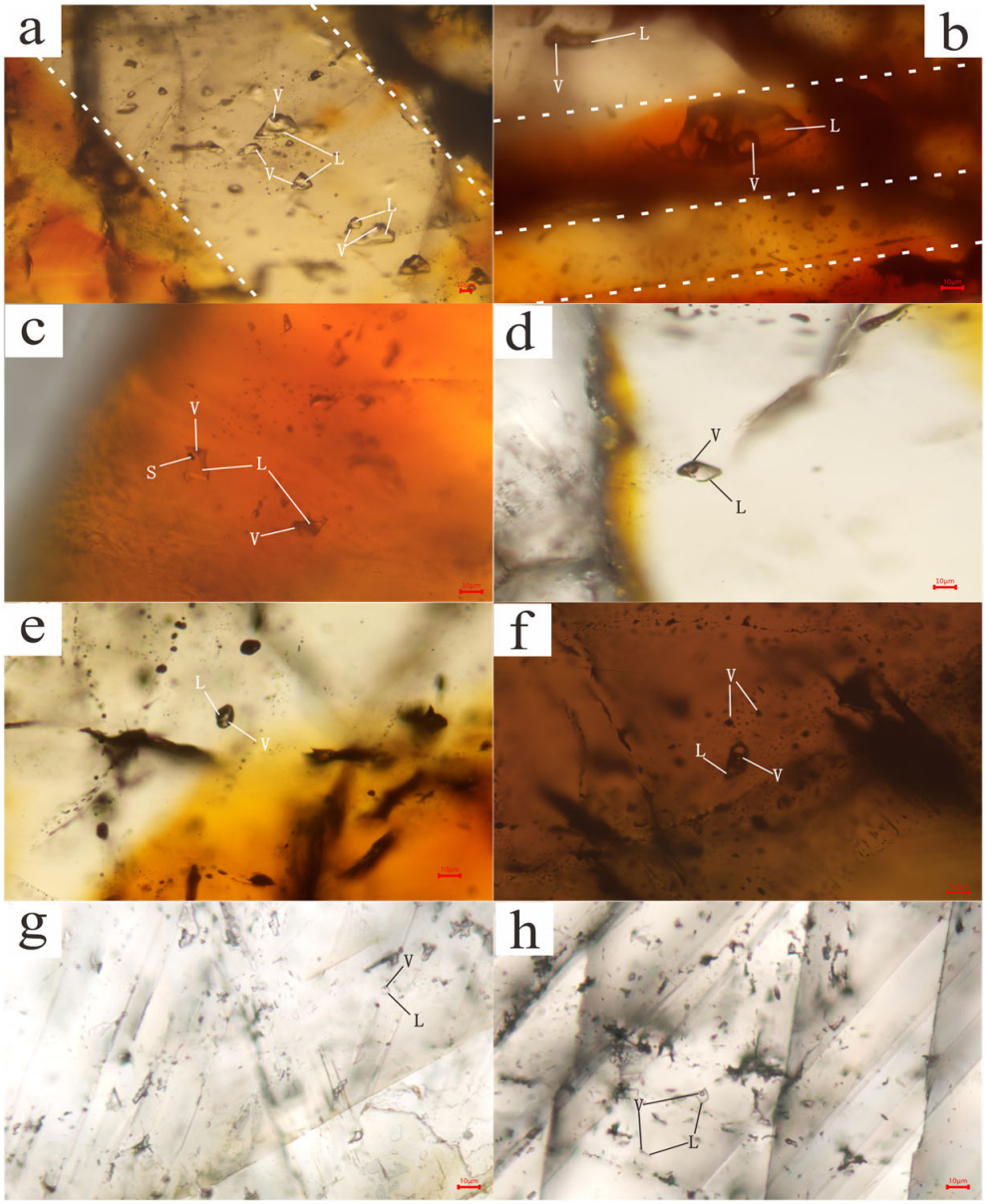

Figure 5. Characteristics of the fluid inclusions in the sphalerite and dolomite of the Fuli Pb-Zn deposits. (**a**,**b**) L + V-type fluid inclusions in Sp-1. (**c**) S + L + V-type fluid inclusion in Sp-1. (**d**,**e**) L+V-type fluid inclusions in Sp-2. (**f**) L+V- and V-type fluid inclusions in Sp-1. (**g**,**h**) L+V-type fluid inclusions in dolomite. Abbreviations: L = liquid; V = vapor; S = solid.

4.2. Microthermometry Results of Fluid Inclusions

By using fluid inclusion microthermometry, temperature and salinity results for the fluid inclusions of the Fuli Pb-Zn deposit were obtained (Table 1), The complete dataset is included in Table S1. The predominant type of fluid inclusions in this deposit is L+V-type inclusions. The temperature measurements indicate that the eutectic temperatures of the fluid inclusions in sphalerite range from −59.1 to −35.5 °C, suggesting the presence of a certain amount of Ca^{2+} and Mg^{2+} in the fluids during this stage [20]. The salinity and homogenization temperatures of the fluid inclusions have a wide range of values, ranging from 182 to 237 °C (mean value: 203 °C) for dolomite, from 117 to 197 °C (mean value: 162 °C) for Sp-1, and from 112 to 171 °C (mean value: 142 °C) for Sp-2. The salinity of the fluid inclusions in dolomite ranges from 4.3 to 9.3 wt.% NaCl Eqv, while for Sp-1, it ranges from 14.3 to 22.8 wt.% NaCl Eqv, and for Sp-2, it ranges from 2.3 to 9.2 wt.% NaCl Eqv. Based on these observations, it can be concluded that the Fuli Pb-Zn deposit is a typical

meso-low-temperature hydrothermal deposit that possibly contains the presence of two types of fluids characterized by low and high salinity (Figure 6).

Table 1. Summary of microthermometric results of fluid inclusions in dolomite and sphalerite in the Fuli deposit.

Mineral	Stage	N	Tm (°C)	Mean Value	Th (°C)	Mean Value	Salinity (wt.% NaCl Eqv.)	Mean Value
dolomite	HD3	21	−2.6 to −6.1	−4.5	182 to 237	203	4.3 to 9.3	7.1
sphalerite	I	31	−10.3 to −20.6	−15.3	117 to 197	162	14.3 to 22.8	18.8
sphalerite	II	17	−1.3 to −6	−3.4	112 to 171	142	2.2 to 9.2	5.5

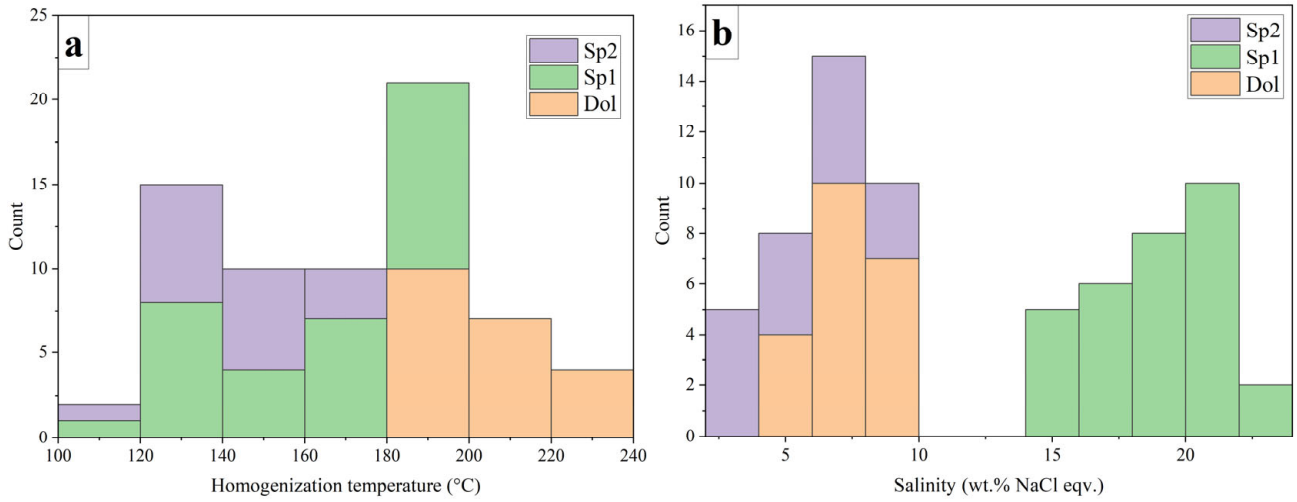

Figure 6. Stacked histograms of fluid inclusion homogenization temperatures (**a**) and salinity (**b**) in the Fuli deposit.

4.3. Laser Raman Characteristics

The fluid inclusions found in the Fuli Pb-Zn deposit primarily consist of two-phase inclusions (L+V-type inclusions). Laser Raman spectroscopy findings have, however, revealed the diverse compositions of the fluid inclusions and subsequently led to the classification of two subtypes, namely Type I and Type II. Type I comprises two-phase gas–liquid inclusions characterized by definite bubble boundaries and an overall transparent colorless appearance (Figure 5a,d). Laser Raman analysis indicates that these inclusions are primarily composed of H_2O, and this type of inclusion is mainly distributed in dolomite. In contrast, Type II two-phase gas–liquid inclusions exhibit black bubbles with rough black margins (Figure 5e). In addition to H_2O, the inclusions also contain CH_4, CO_2, and N_2 (Figure 7); most of the inclusions in sphalerite are Type II inclusions.

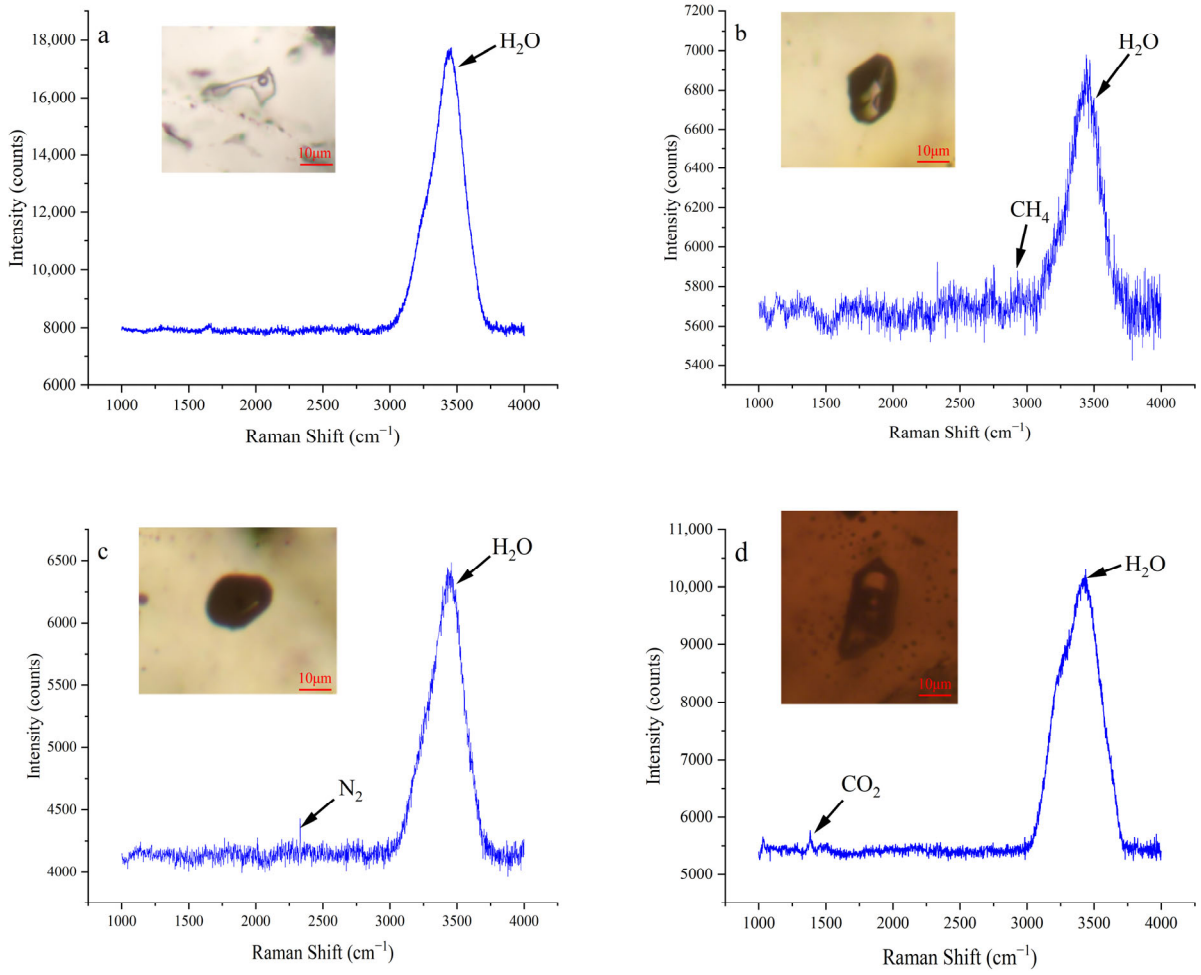

Figure 7. Laser Raman spectra for the fluid inclusions in the sphalerite and dolomite of the Fuli Pb-Zn deposits. (**a**) L + V-type fluid inclusions in dolomite; (**b**,**c**) L + V-type fluid inclusions in Sp-2; and (**d**) L + V-type fluid inclusions in Sp-1.

4.4. H-O Isotopic Analysis

The hydrogen and oxygen isotope compositions obtained from dolomite are listed in Table 2. The $\delta D_{V\text{-}SMOW}$ values range from −49.8 to −96.7‰, with an average value of −65.3‰. The $\delta^{18}O$ values range from +12.1 to +20.8‰, with an average value of +18.9‰.

Table 2. Compositions of hydrogen and oxygen isotopes in dolomite from the Fuli Pb-Zn deposit.

Sample No.	Host	$\delta D_{V\text{-}SMOW}$/‰	$\delta^{18}O_{V\text{-}SMOW}$/‰	T/ °C	$\delta^{18}O_{fluid}$/‰
FL8-1	dolomite	−62.1	20.3	202	10.4
FL8-2	dolomite	−52.4	20.8	202	10.9
FL14	dolomite	−52.8	19.6	202	9.7
FL15	dolomite	−60.3	19.2	202	9.3
FL10	dolomite	−96.7	12.1	202	2.2
FL13	dolomite	−49.8	18.9	202	9

5. Discussion

5.1. Fluid Characteristics

Different fluid systems possess distinct eutectic temperatures. When a fluid keeps a constant composition, the eutectic temperature does not alter with varied concentrations. Thus, it can work as a criterion for identifying the fluid system [20]. The eutectic temperatures for the NaCl-H_2O, $CaCl_2$-H_2O, and $MgCl_2$-H_2O binary systems are −21.2 °C,

−49.8 °C, and −33.6 °C, respectively. The eutectic temperatures for the NaCl-$CaCl_2$-H_2O, NaCl-$MgCl_2$-H_2O, and $CaCl_2$-$MgCl_2$-H_2O ternary systems are −52.0 °C, −35.0 °C, and −55.0 °C, respectively [20]. The fluid inclusions discovered in early-stage minerals like calcite indicate a NaCl-H_2O system, as evidenced by their eutectic temperatures of −21.8 °C and −22.6 °C. Furthermore, the fluid inclusions in sphalerite have an eutectic temperature range of −55.4 °C to −35.8 °C, which suggests a NaCl-$CaCl_2$-H_2O fluid system.

During the initial stage of mineralization, carbonate mineral precipitation leads to a decrease in ion concentration due to the formation of Mg^{2+} and Ca^{2+}, resulting in the dominance of the NaCl-H_2O fluid composition. In the primary mineralization stage, water/rock reactions keep carbonate rocks in a cycle of dissolution and reprecipitation [12], with the main mineralization fluids containing ions like Mg^{2+}, Ca^{2+}, and SO_4^{2-}. This discovery aligns with previous studies on the liquid-phase compositions of neighboring deposits including Daliangzi, Tianbaoshan, Jinding [21,22]. Our laser Raman analysis of the gas phase identified CH_4, CO_2, and N_2, which are often linked to reducing conditions, implying that the mineralizing fluids have reducing properties.

5.2. Fluid Mixing

The Fuli deposit consists of three groups of fluid inclusions with varying homogenization temperatures and salinities, exhibiting a broad range of temperature (112–237 °C) and salinity (2.3–22.8 wt.% NaCl eqv.) variations (Figure 8). These variations are often attributed to fluid mixing during the ore deposition processes [23–26]. The inclusions in the HD3 dolomite demonstrate the properties of metamorphic fluids in terms of both temperature and salinity. The inclusions found in Sp-1 are within the range of basin brines and display a decrease in temperature but a considerable increase in salinity, thus indicating the mixing of new external basin brines with metamorphic fluids.

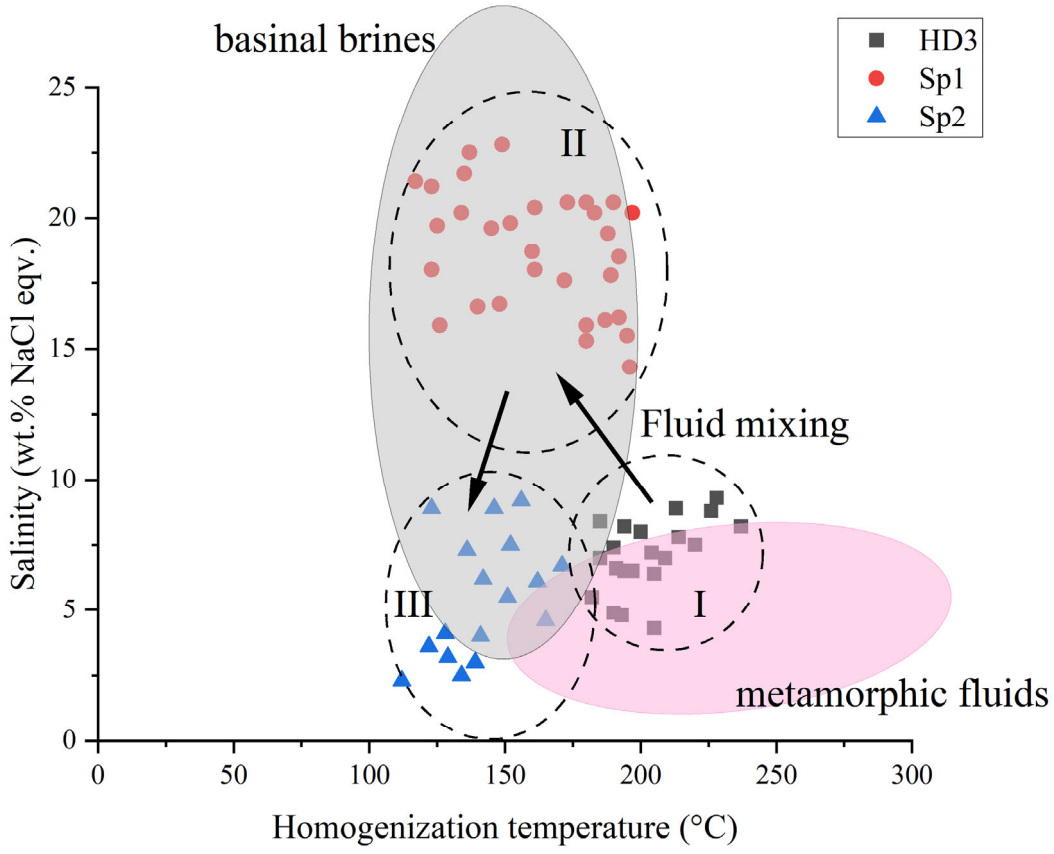

Figure 8. Diagram of homogenization temperatures and salinities of fluid inclusions in different stages of Fuli deposit. I HD3 dolomite, II Sphalerite with high salinity, III Sphalerite with low salinity.

Employing H and O isotopes to trace the origin of ore-forming fluids is a well-known and efficient method in ore deposit research, as fluids deriving from various sources have hydrogen and oxygen isotopes with unique compositions [27–32]. Most of the isotopic data from dolomite fluids in the δD versus $\delta^{18}O_{fluid}$ diagram (Figure 9) lie within the range of metamorphic water, with one data point falling within the range of organic water. A trend towards atmospheric precipitation or basin brines is generally observed in the isotopic data of dolomite fluids, suggesting the mixing of these two fluids.

Although the fluids in the initial mineralization stage are characterized by metamorphic fluids (Figure 8), their high temperatures can also be associated with mantle fluids (or magmatic fluids), particularly given the presence of Emeishan basalt coverage in the study area (Figure 2) [26,33].

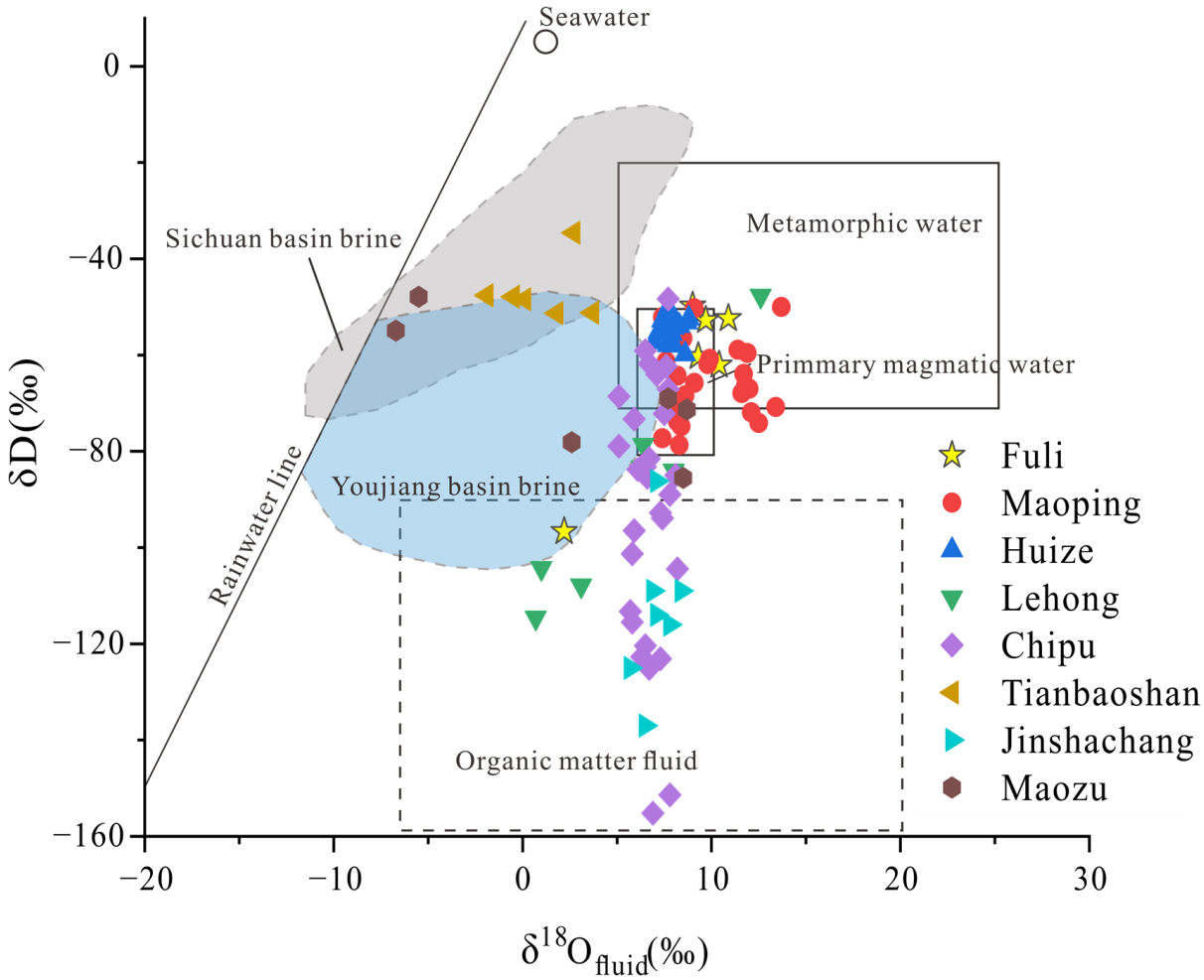

Figure 9. Diagram of δD vs. $\delta^{18}O_{fluid}$ for dolomite from Fuli deposit and some Pb-Zn deposits in SYGMB (modified from Kesleret al. [28], Taylor [34], and Wang et al. [31], respectively). Data from Wang et al. [26], Zhou et al. [35], Zhao et al. [36], Hai et al. [37], Ding et al. [38], Wen et al. [39], Wu et al. [40], Yuan et al. [41], Yuan et al. [42], and Yang et al. [43], The complete dataset is included in Table S2.

5.3. Organic Matter and TSR Interaction

Organic matter is crucial to the formation and evolution of petroleum and natural gas, as well as to the complexation, transportation, unloading, and accumulation of certain metallic elements [44]. Certain geological conditions can lead to the creation of a biotic–organic matter ore-forming fluid system through geological processes. During the formation of the Fuli Pb-Zn deposit, organic fluids were present as significant components of ore-forming fluids during the hydrothermal mineralization stage. The study of the

Pb-Zn deposits near the Fuli deposit also indicate the possibility of organic fluid activity in the study area, as evidenced by the discovery of organic fluids containing asphalt and methane-bearing inclusions (unpublished data).

The association between Pb-Zn minerals and organic matter has been a central focus of research. Fluid inclusions, crucial constituents of ore-forming fluids, provide crucial proof of organic matter's involvement in the mineralization process. Methane inside fluid inclusions can be produced in multiple ways, such as microbial sulfate reduction (BSR) and thermochemical sulfate reduction (TSR). BSR reactions take place at temperatures below 80 °C [45]. Based on the temperature results of the fluid inclusions in this deposit, it can be concluded that BSR reactions are not the primary source of H_2S. Hence, the hypothesis that BSR reactions are the main reason behind CH_4 can be discarded.

If the TSR occurs and provides reduced sulfur for mineralization, sulfur isotope fractionation can be observed. The difference in $\delta^{34}S$ between sulfate minerals and sulfide minerals ($\Delta\delta^{34}S$) is significant, and temperature also influences this difference. For instance, during the TSR, fractionation takes place between seawater sulfate and reduced sulfur. At temperatures of 100 °C, $\Delta\delta^{34}S$ is 20‰; at 150 °C, $\Delta\delta^{34}S$ is 15‰; and at 200 °C, $\Delta\delta^{34}S$ is 10‰ [12,41,45,46]. During sulfide precipitation, there is no noticeable sulfur isotope fractionation between metal sulfides and reduced sulfur. In metallic deposits, the $\delta^{34}S$ values of metal sulfides depend on the reduced S from the TSR and are typically 10% to 20% lower than the $\delta^{34}S$ values of seawater sulfate in the surrounding rocks [2,42,47–49]. At the Fuli Pb-Zn deposit, sulfide minerals including sphalerite, galena, and minor pyrite are present, but no sulfate minerals have been detected. Consequently, the sulfides mean $\delta^{34}S$ value is suitable for representing the $\delta^{34}S_{\Sigma S}$ of the hydrothermal fluids. Fluid inclusion temperature results demonstrate that mineralization temperatures range from 117 °C to 237 °C. If the TSR occurs in the Fuli deposit, the sulfide $\delta^{34}S$ values in the ore should be 10‰ to 20‰ below the seawater sulfate $\delta^{34}S$ values in the surrounding rocks, resulting in a $\Delta\delta^{34}S$ of 10‰ to 20‰. Sulfur isotope testing was carried out on sphalerite samples from the Fuli deposit, revealing $\delta^{34}S$ values ranging from +15.57‰ to +16.91‰, with an average of +16.26‰ [50]. The deposit's sedimentary strata house numerous evaporite gypsum formations, with marine sulfates $\delta^{34}S$ values being concentrated between +20.0‰ and +38.7‰, averaging at +29‰ [51–54]. Compared to the $\delta^{34}S$ values of sulfides found in Fuli ores, a difference in the $\Delta\delta^{34}S$ value of approximately 13‰ implies the presence of the TSR in the Fuli Pb-Zn deposit. This discovery suggests that the TSR played a role in acting as a source of reduced sulfur for mineralization.

5.4. Ore-Forming Mechanism

There is a significant correlation between orogenic belts and sedimentary basins as they depend on each other in terms of spatial distribution and material conversion [55]. The Youjiang Basin, situated on the western edge of the Yangtze Block, forms a composite "basin-mountain system" with the surrounding orogenic belts. This system plays a crucial role in controlling the metallogenic and mineralization processes within the basin [10,11,33]. The Fuli deposit is located on the southwestern margin of the Youjiang Basin, which underwent significant Indosinian orogeny from the Late Triassic to the Early Jurassic. This resulted from the intense compression of the southwestern part of the Yangtze Block [10,56–59]. Due to uplift of the Youjiang Foreland Basin on the Youjiang fold belt, basin brines originating from the Youjiang Basin migrated northwestward towards the southwestern part of the Yangtze Block due to the effects of gravity and/or tectonic forces [4,60]. During the migration of brines from the basin, elements responsible for ore-forming, such as Pb and Zn, were extracted consistently from both cover or basement rocks. This led to the creation of ore fluids presenting higher concentrations of Zn^{2+}, Pb^{2+}, Mg^{2+}, Ca^{2+}, and Cl^- with medium temperature (117–237 °C) and high salinity (14–22.8 wt.% NaCl Eqv). Subsequently, methane (CH_4) from coal-bearing strata widely distributed in the eastern and southeastern portions of the Fuli mining region acted as a reducing agent. This conversion process transformed the SO_4^{2-} obtained from the evaporite gypsum layers in

the geological formations of the mining area into H_2S through the thermochemical sulfate reduction (TSR). The mixing of low-temperature, high-salinity basin brines with high-temperature, low-salinity metamorphic fluids in the Middle Permian Yangxin Formation resulted in mineralization.

The sulfur isotope signatures indicate that the sulfur present in the Fuli deposit originates from seawater sulfate [3,12,50]. The reduction of SO_4^{2-} in seawater can produce the reduced sulfur required for the precipitation of metal sulfides through a series of processes [61]. The high-salinity ore fluids at medium temperature (117–237 °C) provide the SO_4^{2-} required for the TSR. Mg^{2+} serves as a catalyst, accelerating the initiation of the TSR [62,63]. The ore-forming fluids present in the Fuli deposit contain Mg^{2+} (refer to Section 5.1), reaching the threshold temperature of 100–140 °C [45], which is required for the TSR to take place. The addition of CH_4 and H_2S from the coal-bearing strata in the mining region promotes the smooth progression of the TSR [45,64].

When the thermochemical sulfate reduction (TSR) takes place, organic matter serves as the reducing agent that transforms SO_4^{2-} into reduced sulfur [8,45,65–67]. The following equations, Equations (1)–(3) [45,68], represent the possible reactions:

$$4CH_2 + 3SO_4^{2-} + 2H_2O \rightarrow 4CO_2 + 3H_2S + 6OH^- \quad (1)$$

Large amounts of H_2S are produced in the process [69]:

$$CH_4 + SO_4^{2-} \rightarrow CO_3^{2-} + H_2S + 2H_2O \quad (2)$$

$$\text{Organic matter} + SO_4^{2-} \rightarrow \text{Hydrocarbons} + \text{bitumen} + CO_3^{2-} + H_2S + CO_2 + H_2O \quad (3)$$

$$Mg^{2+} + Ca^{2+} + 2CO_2 + 2H_2O \rightarrow CaMg(CO_3)_2\downarrow + 4H^+ \quad (4)$$

$$Zn^{2+} + H_2S \rightarrow ZnS\downarrow + 2H^+ \quad (5)$$

$$2Fe^{3+} + 3H_2S \rightarrow FeS_2\downarrow + FeS\downarrow + 6H^+ \quad (6)$$

$$Pb^{2+} + H_2S \rightarrow PbS\downarrow + 2H^+ \quad (7)$$

Reactions (4)–(7) occur with a large amount of H^+, which changes the pH of the ore-forming fluid, leading to a decrease in the solubility of metal ions, which further promotes the precipitation of minerals.

6. Conclusions

(1) The formation process of the Fuli Pb-Zn deposit can be divided into three stages: (I) the precipitation of hydrothermal dolomite, (II) the precipitation of sphalerite + galena, and (III) the precipitation of calcite. The first stage occurs at a medium temperature (182–237 °C) and in fluids with low salinity (4.3–9.3 wt.% NaCl eqv.). In the early part of the second stage, low to medium temperatures (117–197 °C) and high-salinity (14.3–22.8 wt.% NaCl eqv.) fluids were observed, while the late part of the second stage is characterized by low to medium temperatures (112–171 °C) and low salinity (2.3–9.2 wt.% NaCl eqv.).

(2) Petrographic studies show that the inclusions are two-phase gas–liquid inclusions with complex compositions. Laser Raman spectroscopy showed the presence of components other than H_2O, such as CH_4, N_2, and CO_2. The initial melting temperature of the inclusions indicates that the fluids in the hydrothermal calcite stage consist mainly of a NaCl-H_2O fluid system, while the sphalerite + galena stage contains multiple ions, such as Mg^{2+} and Ca^{2+}, forming a multicomponent fluid system.

(3) The Fuli deposit was formed by the mixture of low-temperature, medium–high salinity basin brine and high-temperature, low-salinity metamorphic fluids, and mineralization occurred in the Middle Permian Yangxin Formation. At an appropriate temperature range (120–260 °C), the sulfate (SO_4^{2-}) carried by the ore-bearing fluid and the catalyst (Mg^{2+}) jointly promote the initiation of TSR, leading to the precip-

itation of metal sulfides. The change in fluid pH during the reduction of sulfate by organic matter and CH_4 further facilitated the precipitation of metal sulfides. The presence of asphalt, CH_4, N_2, CO_2, and sulfur isotope fractionation characteristics in the ore-forming fluids constitute evidence of the occurrence of the TSR.

Supplementary Materials: The following supporting information can be downloaded at: https://www.mdpi.com/article/10.3390/min14030312/s1, Table S1: Results of fluid inclusion analysis from the Fuli Pb-Zn deposit; Table S2: Comparison of the H-O istopic data for carbonate-hosted Pb-Zn deposits in the SYGMB.

Author Contributions: Formal analysis, X.Z.; Investigation, H.Q. and G.L.; Writing—original draft, X.L.; Writing—review & editing, B.L. All authors have read and agreed to the published version of the manuscript.

Funding: This research received no external funding.

Data Availability Statement: All data are contained within the article and Supplementary Materials.

Conflicts of Interest: Author Huaikun Qin and Gao Li was employed by the company Fuli Pb-Zn Mine Co., Ltd., Author Xinyue Zhang was employed by the company Kunming Geological Prospecting Institute, China Metallurgical Geological Bureau. The remaining authors declare that the research was conducted in the absence of any commercial or financial relationships that could be construed as a potential conflict of interest.

References

1. Liu, H.C.; Lin, W.D. *Regularity Research of Ag, Zn, Pb Ore Deposits North-East Yunnan Province*; Yunnan University Press: Kunming, China, 1999.
2. Zhou, J.-X.; Wang, X.-C.; Wilde, S.A.; Luo, K.; Wu, T. New Insights into the Metallogeny of MVT Zn-Pb Deposits: A Case Study from the Nayongzhi in South China, Using Field Data, Fluid Compositions, and in Situ S-Pb Isotopes. *Am. Mineral.* **2018**, *103*, 91–108. [CrossRef]
3. Ren, T.; Zhou, J.; Wang, D.; Yang, G.; Lv, C. Trace Elemental and S-Pb Isotopic Geochemistry of the Fule Pb-Zn Deposit, NE Yunnan Province. *Acta Petrol. Sin.* **2019**, *35*, 3493–3505. [CrossRef]
4. Yang, Q.; Liu, W.; Zhang, J.; Wang, J.; Zhang, X. Formation of Pb-Zn Deposits in the Sichuan–Yunnan–Guizhou Triangle Linked to the Youjiang Foreland Basin: Evidence from Rb-Sr Age and in Situ Sulfur Isotope Analysis of the Maoping Pb-Zn Deposit in Northeastern Yunnan Province, Southeast China. *Ore Geol. Rev.* **2019**, *107*, 780–800. [CrossRef]
5. Xiong, S. Compositions and Microthermometry of Fluid Inclusions of Chalukou Porphyry Mo Deposit from Great Xing an Range:Implications for Ore Genesis. *Earth Sci. J. China Univ. Geosci.* **2014**, *39*, 820–836. [CrossRef]
6. Wilkinson, J.J. Fluid Inclusions in Hydrothermal Ore Deposits. *Lithos* **2001**, *55*, 229–272. [CrossRef]
7. Anderson, G.M. Organic Maturation and Ore Precipitation in Southeast Missouri. *Econ. Geol.* **1991**, *86*, 909–926. [CrossRef]
8. Leach, D.L.; Sangster, D.F.; Kelley, K.D.; Large, R.R.; Garven, G.; Allen, C.R.; Gutzmer, J.; Walters, S. Sediment-Hosted Lead-Zinc DepositsA Global Perspective. In *One Hundredth Anniversary Volume*; Society of Economic Geologists: Tulsa, OK, USA, 2005; ISBN 978-1-887483-01-8.
9. Wu, Y.; Zhang, C.; Mao, J.; Zhang, W.; Wei, C. The Relationship between Oil-Gas Organic Matter and MVT Mineralization: A Case Study of the Chipu Lead-Zinc Deposit, Sichuan. *Acta Geosci. Sin.* **2013**, *34*, 425–436. [CrossRef]
10. Han, R.; Wu, P.; Zhang, Y.; Huang, Z.; Wang, F.; Jin, Z.; Zhou, G.; Shi, Z.; Zhang, C. New Research Progresses of Metallogenic Theory for Rich Zn-Pb-(Ag-Ge) Deposits in the Sichuang-Yunnan-Guizhou Triangle (SYGT) Area, Southwestern Tethys. *Acta Geol. Sin.* **2022**, *96*, 554–573.
11. Han, R.; Yan, Z.; Qiu, W.; Ding, T.; Wang, M.; Feng, W. Geology and Geochemistry of Zn-Pb (-Ge-Ag) Deposits in the Sichuan-Yunnan-Guizhou Triangle Area, China: A Review and a New Type. *Front. Earth Sci.* **2023**, *11*, 1136397.
12. Zhou, J.-X.; Luo, K.; Wang, X.-C.; Wilde, S.A.; Wu, T.; Huang, Z.-L.; Cui, Y.-L.; Zhao, J.-X. Ore Genesis of the Fule Pb Zn Deposit and Its Relationship with the Emeishan Large Igneous Province: Evidence from Mineralogy, Bulk COS and in Situ SPb Isotopes. *Gondwana Res.* **2018**, *54*, 161–179. [CrossRef]
13. Nian, H.; Cui, Y.; Li, Z.; Jia, F.; Yang, S.; Cheng, W.; Yang, Z. Features of Sphalerite-Hosted Fluid Inclusions of Fule Lead-Zinc Mining Area and Outskirts in Luoping Area, Eastern Yunnan Province, China. *ACTA Mineral. Sin.* **2017**, *37*, 469–474. [CrossRef]
14. Xu, C.; Zhong, H.; Zhu, W.; Tang, L.; Song, C.; Luo, G. Characteristics of sulfur, lead, zinc and cadmium isotopes of sphalerites in the Fusheng Pb-Zn deposit in Yunnan Province and their indicative significances. *Acta Mineral. Sin.* **2022**, *42*, 732–744. [CrossRef]
15. Ni, P.; Li, W.; Pan, J. Ore-Forming Fluid and Metallogenic Mechanism of Wolframite–Quartz Vein-Type Tungsten Deposits in South China. *Acta Geol. Sin. Ed.* **2020**, *94*, 1774–1796.

16. Steele-MacInnis, M.; Lecumberri-Sanchez, P.; Bodnar, R.J. HokieFlincs_H_2O-NaCl: A Microsoft Excel Spreadsheet for Interpreting Microthermometric Data from Fluid Inclusions Based on the PVTX Properties of H_2O–NaCl. *Comput. Geosci.* **2012**, *49*, 334–337. [CrossRef]
17. Steele-MacInnis, M.; Bodnar, R.J.; Naden, J. Numerical Model to Determine the Composition of H_2O–NaCl–$CaCl_2$ Fluid Inclusions Based on Microthermometric and Microanalytical Data. *Geochim. Cosmochim. Acta* **2011**, *75*, 21–40. [CrossRef]
18. Zhang, M.; Hu, P.; Niu, Y.; Su, S. Chemical and Stable Isotopic Constraints on the Nature and Origin of Volatiles in the Sub-Continental Lithospheric Mantle beneath Eastern China. *Lithos* **2007**, *96*, 55–66. [CrossRef]
19. Zheng, Y.; Zhou, G.; Gong, B. Theoretical Study on Oxygen Isotope Fractionation in Carbonate Minerals. *Geol. J. China Univ.* **1997**, *3*, 241.
20. Lu, H.; Fan, H.; Ni, P. *Fluid Inclusion*; Science Press: Beijing, China, 2004.
21. Liu, W.; Wang, J.; Li, Z. Geochemical Characteristics of Lead-Zinc Deposits at Eastern Margin of Kangdian Axis. *Miner. Depos.* **2002**, *21*, 173–176. [CrossRef]
22. Mu, L.; Hu, R.; Bi, X.; Tang, Y.; Lan, T.; Lan, Q.; Zhu, J.; Peng, J.; Oyebamiji, A. New Insights into the Origin of the World-Class Jinding Sediment-Hosted Zn-Pb Deposit, Southwestern China: Evidence from LA-ICP-MS Analysis of Individual Fluid Inclusions. *Econ. Geol.* **2021**, *116*, 883–907. [CrossRef]
23. Wilkinson, J. A Review of Fluid Inclusion Constraints on Mineralization in the Irish Ore Field and Implications for the Genesis of Sediment-Hosted Zn-Pb Deposits. *Econ. Geol.* **2010**, *105*, 417–442. [CrossRef]
24. Li, D.-F.; Chen, H.-Y.; Zhang, L.; Hollings, P.; Chen, Y.-J.; Lu, W.-J.; Zheng, Y.; Wang, C.-M.; Fang, J.; Chen, G.; et al. Ore Geology and Fluid Evolution of the Giant Caixiashan Carbonate-Hosted Zn-Pb Deposit in the Eastern Tianshan, NW China. *Ore Geol. Rev.* **2016**, *72*, 355–372. [CrossRef]
25. Nejadhadad, M.; Taghipour, B.; Lentz, D.R. Implications of Multiple Fluids in the Deposition of Pb-Zn-Ba Deposits in the Alvand Mountain, Golpayegan, Iran: Evidence from Fluid Inclusions and O, C, S Isotopes. *Ore Geol. Rev.* **2023**, *153*, 105300. [CrossRef]
26. Wang, L.; Han, R.; Zhang, Y.; Li, X. Mixing in Two Types of Fluids Responsible for Some Carbonate-Hosted Pb-Zn Deposits, SW China: Insights from the Maoping Deposit. *Minerals* **2023**, *13*, 600. [CrossRef]
27. Samson, I.M.; Russell, M.J. Genesis of the Silvermines Zinc-Lead-Barite Deposit, Ireland; Fluid Inclusion and Stable Isotope Evidence. *Econ. Geol.* **1987**, *82*, 371–394. [CrossRef]
28. Kesler, S.E.; Vennemann, T.W.; Frederickson, C.; Breithaupt, A.; Vazquez, R.; Furman, F.C. Hydrogen and Oxygen Isotope Evidence for Origin of MVT-Forming Brines, Southern Appalachians. *Geochim. Cosmochim. Acta* **1997**, *61*, 1513–1523. [CrossRef]
29. Meinert, L.; Hedenquist, J.; Satoh, H.; Matsuhisa, Y. Formation of Anhydrous and Hydrous Skarn in Cu-Au Ore Deposits by Magmatic Fluids. *Econ. Geol.* **2003**, *98*, 147–156. [CrossRef]
30. Xu, R.; Li, W.-C.; Deng, M.-G.; Zhou, J.-X.; Ren, T.; Yu, H.-J. Genesis of the Superlarge Luziyuan Zn-Pb-Fe (-Cu) Distal Skarn Deposit in Western Yunnan (SW China): Insights from Ore Geology and CHOS Isotopes. *Ore Geol. Rev.* **2019**, *107*, 944–959. [CrossRef]
31. Wang, K.; Wang, Y.-H.; Xue, C.-J.; Liu, J.-J.; Zhang, F.-F. Fluid Inclusions and C–H–O–S–Pb Isotope Systematics of the Caixiashan Sediment-Hosted Zn-Pb Deposit, Eastern Tianshan, Northwest China: Implication for Ore Genesis. *Ore Geol. Rev.* **2020**, *119*, 103404. [CrossRef]
32. Zhang, P.; Kou, L.; Zhao, Y.; Sha, D. Genesis of the Maoling Gold Deposit in the Liaodong Peninsula: Constraints from a Combined Fluid Inclusion, C-H-O-S-Pb-He-Ar Isotopic and Geochronological Studies. *Geosci. Front.* **2022**, *13*, 101379. [CrossRef]
33. Zhou, J.-X.; Xiang, Z.-Z.; Zhou, M.-F.; Feng, Y.-X.; Luo, K.; Huang, Z.-L.; Wu, T. The Giant Upper Yangtze Pb-Zn Province in SW China: Reviews, New Advances and a New Genetic Model. *J. Asian Earth Sci.* **2018**, *154*, 280–315. [CrossRef]
34. Tayor, H. The Application of Oxygen and Hydrogen Isotope Studies to Problems of Hydrothermal Alteration and Ore Deposit. *Econ. Geol.* **1974**, *69*, 843–883.
35. Zhou, J.-X.; Bai, J.-H.; Huang, Z.-L.; Zhu, D.; Yan, Z.-F.; Lv, Z.-C. Geology, Isotope Geochemistry and Geochronology of the Jinshachang Carbonate-Hosted Pb-Zn Deposit, Southwest China. *J. Asian Earth Sci.* **2015**, *98*, 272–284. [CrossRef]
36. Zhao, D.; Han, R.; Wang, L.; Ren, T.; Wang, J.; Zhang, X.; Cui, J.; Ding, J. Genesis of the Lehong Large Zinc–Lead Deposit in Northeastern Yunnan, China: Evidences from Geological Characteristics and C–H–O–S–Pb Isotopic Compositions. *Ore Geol. Rev.* **2021**, *135*, 104219. [CrossRef]
37. Wang, H.; Zhu, X.Y.; Wang, J.B.; Jia, D.L.; Shi, Y.; Chen, L.; Xu, Z.F. Sources of Metallogenic Materials and Metallogenic Mechanism of Tianbaoshan Pb-Zn Deposit in Sichuan Province: Constraints from Fluid Inclusions and Isotopic Evidences. *Acta Petrol. Sin.* **2021**, *37*, 1830–1846. [CrossRef]
38. Ding, W.P.; Xie, C.F.; Huang, C.; Zhang, B.; Xin, Z.; Zhan, H.S.; Zheng, L.L.; Kong, F.Q.; Wang, H.B.; Huang, L.F. Sources of Permian Lead-Zine Ore-Forming Materials in Sichuan-Yunnan-Guizhou Area: CHOS-Pb Isotope Constraints—An Example from Taipingzi Lead-Zinc Deposit in Yunnan Provinces. *Geol. China* **2022**, *49*, 1845–1861.
39. Li, W.; Huang, Z.; Zhang, G. Sources of the Ore Metals of the Huize Ore Field in Yunnan Province: Constraints from Pb, S, C, H, O and Sr Isotope Geochemistry. *Acta Petrol. Sin.* **2006**, *22*, 2567–2580.
40. Wu, Y.; Zhang, C.; Mao, J.; Ouyang, H.; Sun, J. The Genetic Relationship between Hydrocarbon Systems and Mississippi Valley-Type Zn-Pb Deposits along the SW Margin of Sichuan Basin, China. *Int. Geol. Rev.* **2013**, *55*, 941–957. [CrossRef]

41. Yuan, B.; Mao, J.; Yan, X.H.; Wu, Y.; Zhang, F.; Zhao, L.L. Sources of Metallogenic Materials and Metallogenic Mechanism of Daliangzi Ore Field in Sichuan Province: Constraints from Geochemistry of S, C, H, O, Sr Isotope and Trace Element in Sphalerite. *Acta Petrol. Sin.* **2014**, *30*, 209–220.
42. Luo, K.; Zhou, J.-X.; Ju, Y. A Shift from BSR to TSR Caused the Formation of the Chipu Pb-Zn Deposit, South China. *Ore Geol. Rev.* **2022**, *144*, 104845. [CrossRef]
43. Yang, Q.; Zhang, J.; Wang, J.; Zhong, W.; Liu, W. Study of Ore-Forming Fluid Geochemistry of Maozu Large-Scale Lead-Zinc Deposit in Northeast Yunnan. *Miner. Resour. Geol.* **2017**, *31*, 854–863.
44. Li, R.X.; Dong, S.W.; Zhang, S.N.; Zhu, R.J.; Xia, B. Features and Formation of Organic Fluids during Dabashan Orogenesis. *J. Nanjing Univ. Nat. Sci.* **2012**, *48*, 295–307. [CrossRef]
45. Machel, H.G. Bacterial and Thermochemical Sulfate Reduction in Diagenetic Settings—Old and New Insights. *Sediment. Geol.* **2001**, *140*, 143–175. [CrossRef]
46. Machel, H.G.; Krouse, H.R.; Sassen, R. Products and Distinguishing Criteria of Bacterial and Thermochemical Sulfate Reduction. *Appl. Geochem.* **1995**, *10*, 373–389. [CrossRef]
47. Liu, W.-H.; Zhang, J.; Wang, J. Sulfur Isotope Analysis of Carbonate-Hosted Zn-Pb Deposits in Northwestern Guizhou Province, Southwest China: Implications for the Source of Reduced Sulfur. *J. Geochem. Explor.* **2017**, *181*, 31–44. [CrossRef]
48. Chen, X.; Xue, C. Origin of H2S in Uragen Large-Scale Zn-Pb Mineralization, Western Tien Shan: Bacteriogenic Structure and S-Isotopic Constraints. *Acta Petrol. Sin.* **2016**, *32*, 1301–1314.
49. Ren, S.; Li, Y.; Zeng, P.; Qiu, W.; Fan, C.; Hu, G. Effect of Sulfate Evaporate Salt Layer in Mineralization of the Huize and Maoping Lead-Zinc Deposits in Yunnan: Evidence from Sulfur Isotope. *Acta Geol. Sin.* **2018**, *92*, 1041–1055.
50. Liang, X.; Li, B.; Zhang, X.; Qin, H.; Li, G.; Zhang, C. Trace Element Composition and Genesis Mechanism of the Fuli Pb-Zn Deposit in Yunnan: LA-ICP-MS and in Situ S-Pb Isotopic Constraints. *Front. Earth Sci.* **2023**, *11*, 1104631. [CrossRef]
51. Huang, Z.L.; Chen, J.; Han, R.S.; Li, W.B.; Liu, C.Q.; Zhang, Z.L.; Ma, D.Y.; Gao, D.R.; Yang, H.L. *Geochemistry and Ore-Formation of the Huize Giant Lead-Zinc Deposit, Yunnan Province, China:Discussion on the Relationship between Emeishan Flood Basalts and Lead-zinc Mineralization*; Geological Publishing House: Beijing, China, 2004.
52. Zhou, J.X.; Huang, Z.L.; JG, G.; Yan, Z.F. Geological and C-O-S-Pb-Sr Isotopic Constraints on the Origin of the Qingshan Carbonate-Hosted Pb-Zn Deposit, Southwest China. *Int. Geol. Rev.* **2013**, *55*, 904–916. [CrossRef]
53. Zhou, J.; Huang, Z.; Zhou, M.; Li, X.; Jin, Z. Constraints of C–O–S–Pb Isotope Compositions and Rb–Sr Isotopic Age on the Origin of the Tianqiao Carbonate-Hosted Pb-Zn Deposit, SW China. *Ore Geol. Rev.* **2013**, *53*, 77–92. [CrossRef]
54. Jin, Z.; Zhou, J.; Zhilong, H.; Luo, K.; Jianguo, G.; Song, P.; Bing, W.; Xinglong, C. Ore Genesis of the Nayongzhi Pb-Zn Deposit, Puding City, Guizhou Province, China: Evidences from S and in Situ Pb Isotopes. *Acta Petrol. Sin.* **2016**, *32*, 3441–3455.
55. Cloetingh, S.; Thybo, H.; Faccenna, C. TOPO-EUROPE: Studying Continental Topography and Deep Earth—Surface Processes in 4D. *Tectonophysics* **2009**, *474*, 4–32. [CrossRef]
56. Wang, C.; Bagas, L.; Lu, Y.; Santosh, M.; Du, B.; McCuaig, T.C. Terrane Boundary and Spatio-Temporal Distribution of Ore Deposits in the Sanjiang Tethyan Orogen: Insights from Zircon Hf-Isotopic Mapping. *Earth-Sci. Rev.* **2016**, *156*, 39–65. [CrossRef]
57. Liu, S.; Zhang, Y.; Ai, G.; Xue, X.; Li, H.; Shah, S.A.; Wang, N.; Chen, X. LA-ICP-MS Trace Element Geochemistry of Sphalerite: Metallogenic Constraints on the Qingshuitang Pb-Zn Deposit in the Qinhang Ore Belt, South China. *Ore Geol. Rev.* **2022**, *141*, 104659. [CrossRef]
58. Wu, Y.; Kong, Z.; Chen, M.; Zhang, C.; Cao, L.; Tang, Y.; Yuan, X.; Zhang, P. Trace Elements in Sphalerites from the Mississippi Valley-Type Lead-Zinc Deposits around the Margins of Yangtze Block and Its Geological Implications: A LA-ICPMS Study. *Acta Petrol. Sin.* **2019**, *35*, 3443–3460. [CrossRef]
59. Liu, X.; Chen, F.; Chang, H.; Gao, J.; Wu, P.; Tan, J. The Mineralization of Daxiao Carbonate-Hosted Pb-Zn Deposit, Northeast Yunnan Province, SW China: Constraints from Rb-Sr Isotopic Dating and H O S-Pb Isotopes. *Ore Geol. Rev.* **2022**, *147*, 104956. [CrossRef]
60. Zhang, C.; Wu, Y.; Hou, L.; Mao, J. Geodynamic Setting of Mineralization of Mississippi Valley-Type Deposits in World-Class Sichuan–Yunnan–Guizhou Zn-Pb Triangle, Southwest China: Implications from Age-Dating Studies in the Past Decade and the Sm–Nd Age of Jinshachang Deposit. *J. Asian Earth Sci.* **2015**, *103*, 103–114. [CrossRef]
61. Sangster, D.F. The Role of Dense Brines in the Formation of Vent-Distal Sedimentary-Exhalative (SEDEX) Lead–Zinc Deposits: Field and Laboratory Evidence. *Miner. Deposita* **2002**, *37*, 149–157. [CrossRef]
62. Tang, Y.; Ellis, G.; Zhang, T.; Jin, Y. Effect of Aqueous Chemistry on the Thermal Stability of Hydrocarbons in Petroleum Reservoirs. *Geochim. Cosmochim. Acta Suppl.* **2005**, *69*, 559.
63. Zhang, S.; Shuai, Y.; He, K.; Mi, J. Research on the Initiation Mechanism of Thermochemical Sulfate Reduction (TSR). *Acta Petrol. Sin.* **2012**, *28*, 739–748.
64. Seewald, J.S. Organic–Inorganic Interactions in Petroleum-Producing Sedimentary Basins. *Nature* **2003**, *426*, 327–333. [CrossRef] [PubMed]
65. Anderson, G. Precipitation of Mississippi Valley-Type Ores. *Econ. Geol.* **1975**, *70*, 937–942. [CrossRef]
66. Ghazban, F.; Schwarcz, H.P.; Ford, D.C. Carbon and Sulfur Isotope Evidence for in Situ Reduction of Sulfate, Nanisivik Lead-Zinc Deposits, Northwest Territories, Baffin Island, Canada. *Econ. Geol.* **1990**, *85*, 360–375. [CrossRef]
67. Jochum, J. Variscan and Post-Variscan Lead-Zinc Mineralization, Rhenish Massif, Germany: Evidence for Sulfide Precipitation via Thermochemical Sulfate Reduction. *Miner. Deposita* **2000**, *35*, 451–464. [CrossRef]

68. Worden, R.H.; Smalley, P.C.; Oxtoby, N.H. The Effects of Thermochemical Sulfate Reduction upon Formation Water Salinity and Oxygen Isotopes in Carbonate Gas Reservoirs. *Geochim. Cosmochim. Acta* **1996**, *60*, 3925–3931. [CrossRef]
69. Mougin, P.; Lamoureux-Var, V.; Bariteau, A.; Huc, A.Y. Thermodynamic of Thermochemical Sulphate Reduction. *J. Pet. Sci. Eng.* **2007**, *58*, 413–427. [CrossRef]